J Therm Spray Tech
https://doi.org/10.1007/s11666-020-01087-6

PEER REVIEWED

Study on Deposition Behavior of Less Than 5 µm YSZ Particles in VLPPS

Jiu-Tao Gao[1] · Lu-Xun Cheng[1] · Yue-Peng Wang[1] · Chang-Jiu Li[1] · Cheng-Xin Li[1]

Submitted: 5 April 2020 / in revised form: 4 July 2020

Abstract A particular YSZ feedstock for very low-pressure plasma spraying (VLPPS) has been designed which can be automatically divided into less than 5 µm YSZ molten particles in the long plasma jet. Fully molten particles were deposited on the substrate at different deposition distances of 250, 350 and 450 mm, respectively. The deposition behavior of less than 5 µm YSZ molten particles were studied aiming to obtain a thin gastight YSZ coating. The flattening ratio of particles at different deposition distances and the gas permeability of YSZ coating prepared by VLPPS were investigated. The results revealed that the thickness of flattened particles was about 0.10-0.35 µm and the flattening ratio of molten particles was about 4.7. The flattened particles were bonded well with substrates and the width of vertical cracks appeared in flattened particles was 0.01-0.02 µm. The gas permeability of coatings prepared at 350 mm was 1.5×10^{-7} cm^4 $(gf)^{-1}$ s^{-1}.

Keywords gastight · splat · very low-pressure plasma spray (VLPPS) · YSZ coating

Introduction

Plasma spraying is a thermal spray process in which molten particles are propelled through a flow of plasma jet to be deposited on a substrate (Ref 1-4). The stacking of individual flattened particles on the substrate develops a coating which tremendously improves service properties of parent materials such as increased corrosion resistance, high temperature working ability or special functions. This technology is well known due to its economic and highly efficient properties (Ref 5-7). Thus, plasma spraying is widely used in many industries such as gas turbines, petrochemical industry and solid oxide fuel cell (SOFC) (Ref 2, 3, 5, 7-9).

In this modern era needs energy without any kind of pollution. In this purposes SOFC serves efficient source of energy which offers numerous advantages like, availability of fuel, flexibility of fuel, low pollution, clean energy, longer service life, more efficiency (Ref 10-17). However, the commercialization of SOFCs is prevented due to the high operating temperatures (>800 °C) which leads to the issues of long-term degradation and instability (Ref 4, 11, 18). SOFC requires higher operating temperatures therein because the conductivity of the electrolyte material decreases at low temperatures. Generally, the ohmic resistance of SOFC is caused by electrolyte layer (Ref 10, 19, 20). Therefore, it is important to prepare a thin and gastight electrolyte layer to reduce the ohmic losses when operating at lower temperature. Post sintering and densification processes are commonly used to obtain a thin gastight ceramic coating prepared by plasma spraying (Ref 21). However, these processes have a negative effect on the electrolyte interface. It is necessary to develop a new method that can be directly used to prepare thin gastight ceramic coatings by plasma spraying.

In general, the microstructure of ceramic coatings prepared by plasma spraying includes many voids, cracks, and crack-free interfaces, which are the reasons for many open interconnect holes in their interiors (Ref 2, 3, 22, 23). It's difficult to guarantee gas tightness when the thickness of the coating is less than 250 µm, (Ref 24). High-velocity

✉ Cheng-Xin Li
licx@mail.xjtu.edu.cn

[1] State Key Laboratory for Mechanical Behavior of Materials, School of Materials Science and Engineering, Xi'an Jiaotong University, Xi'an, Shaanxi, China

Published online: 09 September 2020

oxy-fuel spraying (HVOF) is also used to prepare ceramic coatings (Ref 25, 26). However, defects in the coatings prepared by HVOF are like those in APS. It has been reported that when the diameter of the feedstock powder is reduced from 45 μm to less than 10 μm, thin gas tight ceramic coatings can be prepared by plasma spraying (Ref 5, 9, 24, 27). However; when the powder is less than 10 μm in diameter, feeding it into the center of the plasma jet is still a challenge (Ref 24).

VLPPS is a new technology that developed in recent years, that combines the high deposition efficiency of atmospheric plasma spraying (APS) (Ref 3, 28) and the high strain tolerance of electron beam-physical vapor deposition (EB-PVD) (Ref 29-31). The difference between VLPPS and conventional plasma spraying is that the working pressure of VLPPS is as low as 100 Pa. In this situation, the plasma jet is expanded, and powders, which are designed such as Metco 6700 agglomerated YSZ powders, can be heated to be vaporized in the long plasma jet (Ref 32). Therefore, specific feedstock can be designed to achieve the deposition of small size particles, thereby obtaining a thin, gastight ceramic coating. Currently, researchers have conducted many related studies on how to use this system to prepare columnar structure of YSZ TBC through vapor deposition and cluster deposition (Ref 33-35). Many studies have shown that coatings of different structures can be prepared by adjusting spraying parameters (Ref 36-38). However; the columnar structure of the coating is beneficial to improve the stress resistance of the thermal barrier coating and is not conducive to the thinness and gas-tightness of the coatings.

In this study, a special YSZ agglomeration material was designed for VLPPS. Deposition of completely molten particles less than 5 microns were deposited on the substrate at different spraying distances. In order to obtain a thin, gastight YSZ coating, the deposition behavior of small molten particles was investigated. The flattening ratio of individual particles and the gas permeability of YSZ coatings were measured.

Materials and Experiments

The YSZ (3-mol.% yttria stabilized zirconia) powder was designed by Qingdao Tianyao Industrial Co., Ltd. In order to improve the melting powder of the particles, a soft agglomeration method was used to prepare the powder, and the size of the raw powders was less than 5 μm. The agglomerated powder particle size ranges from 30 to 70 μm. As shown in Fig. 1.

80 kW class power plasma spraying system (MF-P 1000 APS/VPS, GTV, Germany) was used which was placed in a vacuum chamber (10 m^3). During the experiment, the temperature was monitored by a thermal infrared imager (A615, FLIR, USA). YSZ wafers were placed as shown in Fig. 2, which were separated by an equal distance. They were grinded, polished and cleaned. The substrate preheating was carried out through moving the plasma jet without powder feed. The substrate preheating temperature was controlled by varying the number of passes. The deposition of individual particle was achieved by adjusting the plasma gun travel speed and the amount of powder feed. The experimental parameters are shown in Table 1.

The surface morphology of individual particles was observed by field emission scanning electron microscopy (MIRA3 LMH, TESCAN, Czech Republic). The interface between flattened particles and substrates was also observed. The flattening ratio of individual particles was measured and calculated. The flattening ratio of particle was analyzed by using 3D laser microscope (VK9700K, KEYENCE Corporation, Japan) to measure the volume of flattening particles and assuming that the molten droplet particles were ideally spherical. It is easy to get the size of droplet diameters according to the volume of flattening particles. The schematic diagram is shown in Fig. 3(a). At each spraying distance, five different diameter size ranges of flattened particles were statistically analyzed, so the relationship between the diameters of flattened particles and the diameters of molten particles can be gotten. Coatings were prepared on NiO/YSZ wafers (the thickness: 1 mm, the diameter: 20 mm) at the spraying distance of

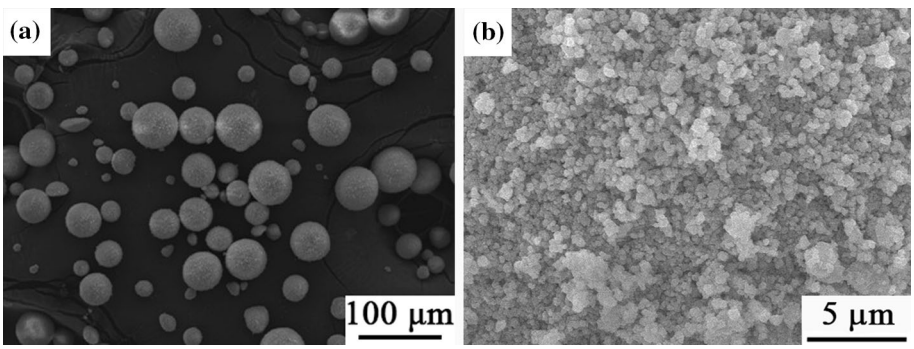

Fig. 1 Morphology of powders used in this experiment: (a) low magnification; (b) high magnification

350 mm. Before measuring the gas permeability of the coating, the sample was reduced in an H_2 atmosphere at 750 °C for 2 h. The schematic diagram of gas-tightness experiment is shown in Fig. 3(b).

The gas permeability can be expressed as (Ref 21):

$$k = \frac{\delta}{A \cdot P_0} \cdot \frac{[\Delta p(t) - \Delta p(t_0)] \cdot V}{\int_{t_0}^{t} \Delta p(t) \mathrm{d}t} \quad \text{(Eq 1)}$$

where k is the gas permeability of the coating (cm^4 $(gf)^{-1}$ s^{-1}), δ is the thickness of the coating (cm), P_0 is the standard atmosphere (Pa), V is the inside volume of the experimental equipment (cm^3) and Δp is the pressure difference ((gf) cm^{-2}).

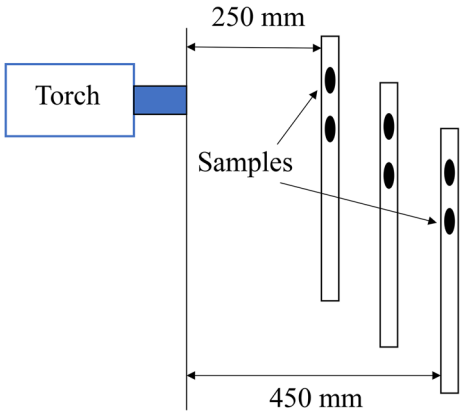

Fig. 2 Schematic representation of the experiment

Table 1 The experimental parameters

Parameter	Value
Arc power, kW	60
Arc current, A	680
Plasma gas (Ar) flow, L min^{-1}	60
Plasma gas (H_2) flow, L min^{-1}	10
Powder feeding gas (Ar) flow, L min^{-1}	2
Chamber pressure, Pa	100
Spraying distance, mm	250/350/450
Torch traverse speed, mm s^{-1}	200

Results and Discussion

Surface Morphology of Flattened YSZ Individual Particles

To prevent severe evaporation, a spray power of 60 kW was used. Before depositing particles, the plasma jet was moved to substrates were preheated by moving the plasma torch to sweep. The surface morphology of YSZ individual particles at different spraying distances is shown in Fig. 4. Figure 4(a) shows the morphology of individual particles at 250 mm. The shapes of these flattened particles are like a disk and the diameters are less than 10 μm. Figure 4(b) and (c) show the surface morphologies of individual particles at 350 and 450 mm, respectively. The shapes and sizes of these particles are similar, as shown in Fig. 4(a).

From above figures, it can be found that small size droplets are deposited on the substrates by VLPPS through a special feedstock design. The size of these flattened particles is much smaller than the size of original powders. This indicates that small particle deposition is realized by feedstock design. During inflight in the plasma jet, the agglomerated powders are exploded into small ones. These small particles are further heated until they are deposited on the substrate. To learn more about particle deposition behavior, particles were deposited on different temperature substrates at 350 mm. The temperatures of substrates were measured by thermal infrared imager. Figure 5 shows the morphology of individual particles at different substrate temperatures: 51, 203, 390, 620 and 735 °C, respectively. When the substrate temperature is low (51 °C), the morphology of the particles is irregular (Fig. 5a and b) and the flattened particles are splashed. With the increase of the substrate temperature (203 °C), the splashing phenomenon

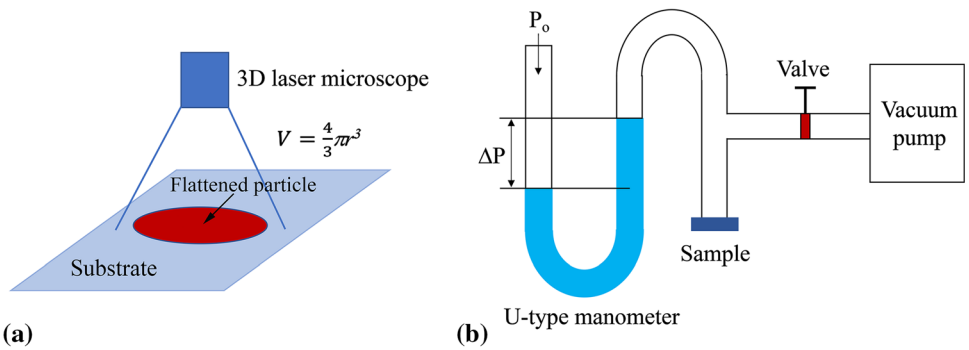

Fig. 3 Schematic representation of: (a) 3D laser microscope; (b) the experimental equipment for gas permeability measurement

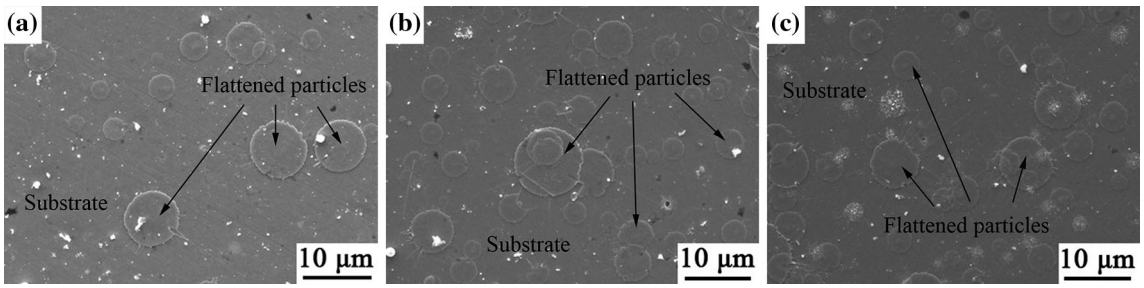

Fig. 4 The morphology of YSZ individual particles at different spraying distances: (a) 250 mm; (b) 350 mm, (c) 450 mm

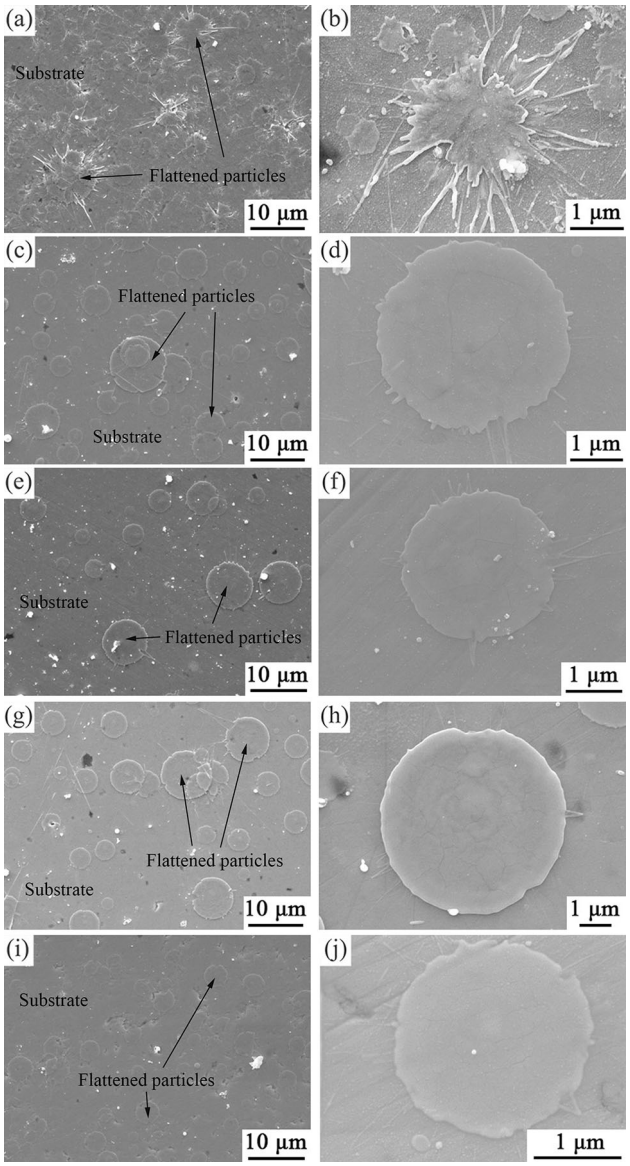

Fig. 5 Morphology of YSZ individual particles at different substrate temperatures: (a), (b) 51 °C; (c), (d) 203 °C; (e), (f) 390 °C; (g), (h) 620 °C; (i), (j) 735 °C

weakened, and the morphology of individual particles begin to show a regular disc shape structure as shown in (Fig. 5c and d). When the temperature of the substrate is higher than 203 °C, the splashing phenomenon becomes significantly less. As the substrate temperature reaches 735 °C, this phenomenon disappears as shown in (Fig. 5i and j). One explanation for this phenomenon is that at low temperatures, organic matter or water will be adsorbed on the surface of the sample, and these organic matter or water will quickly evaporate under the action of high-temperature particles, causing the particles to splash (Ref 39, 40). When the substrate is heated above a certain temperature, such substances will be removed completely. Therefore, the droplet particles are not affected by these substances during the flattening process and a disk-like shape can be obtained. Many studies have also shown that the Reynolds number has a very important effect on the flattening process of droplets, which affects the morphology of the flattened particle (Ref 3, 41, 42). In a certain range with the Reynolds number increased, the morphology of the flattening particle will transform from disc-like to splashed, and a connection also exists between the flattening ratio and Reynolds number.

Interface Between Flattened Particle and Substrate

Figure 6 shows the interface between flattened particle and substrate at different substrate temperatures: 51, 203, 390, 620 and 735 °C, respectively. Due to the low substrate temperature (51 °C), the splashing phenomenon is serious. Although the flattened particle is very small yet it still creates the bond formation with the substrate as shown in (Fig. 6a and b). When the temperature of substrate is preheated to 203 °C, the entire flattened particle is tightly bounded to the substrate as shown in Fig. 6(c). Columnar grains inside flat particles can be observed from higher magnification cross-sectional photograph (Fig. 6b). These columnar grains are perpendicular to the surface of the substrate and penetrate throughout the whole flattened particle, which is well bonded to the substrate. As the substrate temperature increases, the entire flattened particle has a good bonding with the substrate surface. By observing and analyzing, it can be found that the flattened YSZ particles and the substrate produce an effective combination at all experimental temperatures. The

thickness of the flattened particles is about 0.10-0.35 μm. A thin flattened particle is easier to combine with the substrate (Ref 43, 44). Due to the long spraying distance, the droplets are at a high temperature level, which is beneficial for the combination between flattened particles and the substrate (Ref 45).

Deposition Behavior of Small Molten Particles

The size distribution of flattened particles can be different at 250, 350 and 450 mm spraying distances and it affects the microstructure of the coatings: smaller the size of the flattened particles, denser the coating will be (Ref 9). The size distribution of the flat particles at different spraying distances is shown in Fig. 7. At 250 mm, the number of flattened particles diameters less than 10 μm accounts for 83.2% of the fattening particle total number; the diameters between 10 and 20 μm is about 10.1%; the rest only 6.7%. It can be found that the size distribution of the flattened particles is basically similar. Majority of the flattened particles are smaller than 10 μm in diameter, and particles larger than 10 μm are only 16.8, 4.2, and 4% at 250, 350 and 450 mm, respectively, which indicates that most individual particles under the power of 60 kW deposited by VLPPS are less than 10 μm.

The relationship between splat diameter and splat thickness at different spraying distances is shown in Fig. 8. There is an approximately linear relationship between diameter and thickness regardless of the spraying distance. When the diameter of flattening particle is 5 μm, its thickness is about 75 nm; and the diameter of flattening particle 50 μm, its thickness about 350 nm. This means that the greater the diameter of flattening particle is, the thicker it is.

The flattening ratio is the diameter of flattening particle to the diameter of molten particle, which is very important for studying the nature of particle spreading phenomenon and the combination between flattened particle and substrate. Figure 9 shows that when the size of droplet diameter at 250 mm is 1.5 μm, the diameter of flattened particle is 5 μm; the diameter of droplets is 11 μm, the diameter of flattened particles is 50 μm, so the flattening ratio is about 4.7. The similar relationship can be also found and the values of the flattening ratio at 350 and 450 mm are about 4.6 and 4.7, respectively. By analyzing Fig. 9, there is a similar linear relationship between the droplet diameter and the flattened particle diameter at different spraying distances. The slope of curves is almost the same for any

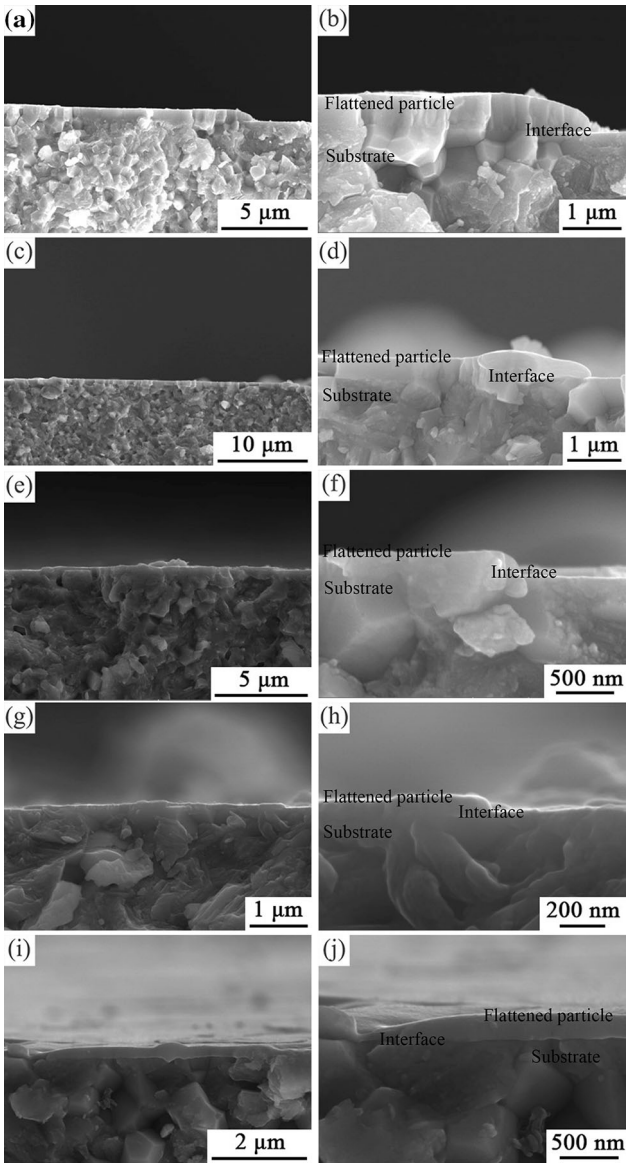

Fig. 6 Interface between flattened and substrate at different substrate temperature: (a), (b) 51 °C; (c), (d) 203 °C; (e), (f) 390 °C; (g), (h) 620 °C; (i), (j) 735 °C

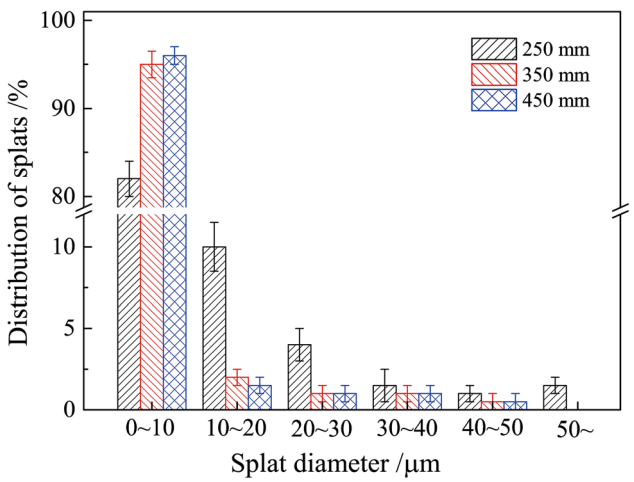

Fig. 7 Distribution of flattened particles at different spraying distances

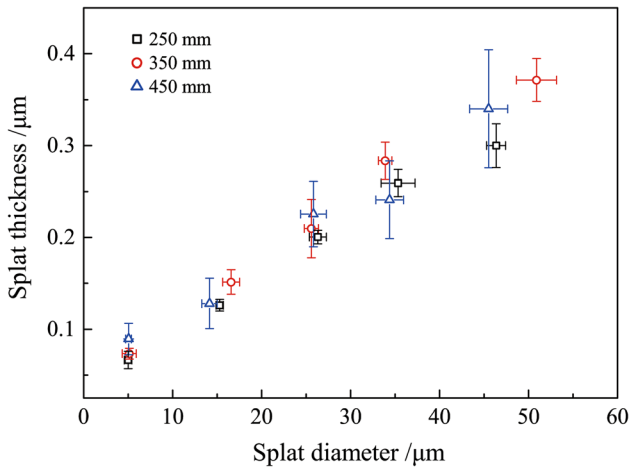

Fig. 8 The relationship between splat diameter and splat thickness at different spraying distances

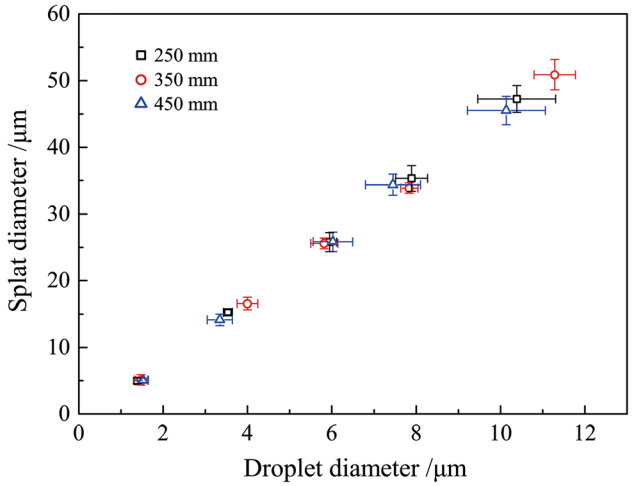

Fig. 9 The relationship between droplet diameter and splat diameter at different spraying distances

distance, i.e. 4.7. This means that the flattening ratio of individual particles prepared by VLPPS does not vary significantly between the spraying distance of 250 to 450 mm. As mentioned above, the plasma jet is greatly expanded under low pressure. The effect of the plasma jet on the particle temperature and velocity may tend to stabilize within a certain distance due to the long infight process. In this case, the spreading ability of the droplets on the substrate is nearly identical. So, the flattening ratio remains the same within the spraying distance of 250-450 mm.

The flattening ratio of flattened particles deposited by several methods (including Atmospheric Plasma Spray (APS) (Ref 1, 2, 46, 47), suspension plasma spray (SPS) (Ref 48, 49), solution precursor plasma spray (SPPS) (Ref 49)) are compared for a more accurate analysis. Figure 10 shows the values of flattening ratio deposited by different

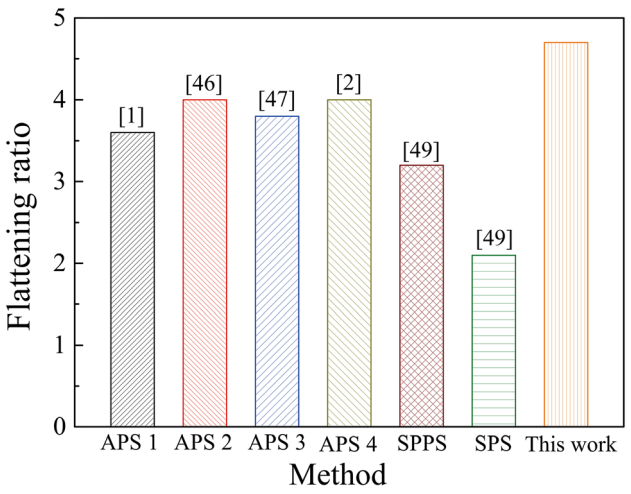

Fig. 10 The comparison chart of the flattening ratio of particles deposited by different methods

methods. The flattening ratio in this work is greater than the flattening ratio under APS or other methods. The greater flattening ratio of the particles indicates the higher spreading ability of the droplets. Increasing the bonding area is useful to reduce the pores between the flattened particles, which can improve the density of coatings (Ref 50).

Many studies have shown that flattened particles have connected vertical cracks (Ref 4, 41, 42, 47, 51-53). Crack width decreases with increasing substrate temperature. The average width of the cracks is about 0.3 μm. When the substrate temperature is 530 °C, the equivalent diameter of the fragments separated by the connected cracks is about 5 μm (Ref 51-53). It is well known that a coating prepared by plasma spraying often exhibits a layered structure. The characteristic of the coating depends on the deposition of individual splats (Ref 54). Therefore, in order to have a better understanding of individual splats contribution to the structure of the plasma sprayed coating, the relationship between splat diameter, fragment equivalent diameter, crack width, and deposition temperature is compared between different methods. Figure 11 shows the relationship between splat diameter, fragment equivalent diameter, crack width, and deposition temperature derived from different studies. Compared with other reported results, the width of cracks in splats deposited in this work is much smaller as well as the equivalent diameter of fragments. It is beneficial to form dense coatings, and consequently, to improve the gastight ability. Li et al. (Ref 27, 51) have reported that, when ceramic particles are deposited by using conventional plasma spraying, deposition temperature significantly affects the interface bond between flattened particles and the substrate. However, in this work, small size flattened particles can bond well with the

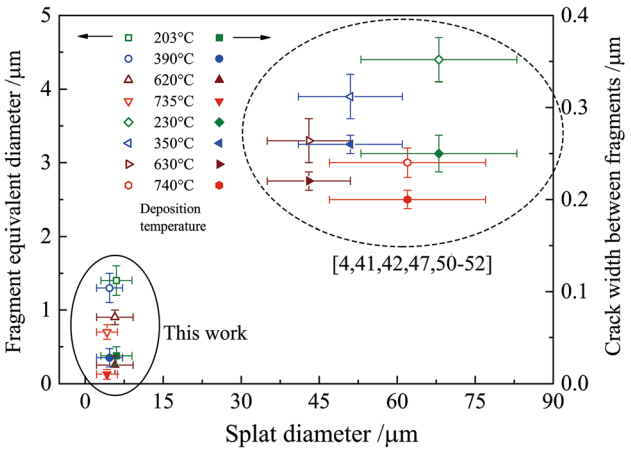

Fig. 11 The relationship between splat diameter, fragment equivalent diameter, crack width, and deposition temperature

substrate and the influence of the deposition temperature on bonding between flattened particles and the substrate is not so strong. This phenomenon may occur due to the deposition of small size particles.

Gas Tightness of YSZ Coatings

Some researchers have reported the gas permeability of coatings prepared by APS (Ref 21, 50), SPS (Ref 55), EB-PVD (Ref 30) and low-pressure plasma spraying (LPPS) (Ref 8) are 15-90 $\times 10^{-7}$, 9.02 $\times 10^{-7}$, 9.78 $\times 10^{-7}$and 6.62 $\times 10^{-7}$ cm^4 $(gf)^{-1}$ s^{-1} respectively. In this work, the gas permeability of coatings at 350 mm is 1.5×10^{-7} cm^4 $(gf)^{-1}$ s^{-1} which is much smaller than others. Figure 12 shows the gas permeability values of ceramic coatings prepared by different techniques. The gas permeability of the coating in this work is as low as the one prepared by APS after 10 densification cycles (1.0×10^{-7} cm^4 $(gf)^{-1}$ s^{-1}).

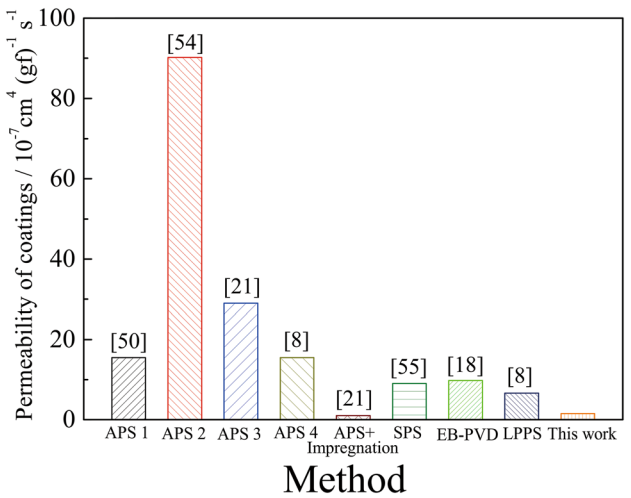

Fig. 12 The permeability of coatings prepared by different methods

Compared to other methods are obvious, the advantage is obvious. It has been reported that the gas permeability practically required for YSZ electrolyte in SOFCs is less than 1.0×10^{-6} cm^4 $(gf)^{-1}$ s^{-1} (Ref 29). This shows that the coating prepared in this work is very suitable to use as an electrolyte layer.

In general, coatings prepared by conventional plasma spraying have a large number of voids, cracks, and non-bonded interfaces. Therefore, the value of gas permeability is usually high when the coating thickness is lower than 250 μm (Ref 24). Figure 13 shows that the structure of the coating prepared by VLPPS is dense and there are few cracks and non-bonded interfaces. The thickness of the coating is about 7 μm and, as aforementioned we know, the thickness of splats is<0.35 μm (as shown in Fig. 6). There are no unbonded interfaces observed in the coating, indicating the effective bonding was formed through several splats. It can be considered that such microstructure of coatings is formed by the growth of the grains of previously deposited splats in contact with solidifying liquid splats through heterogeneous nucleation (Ref 19, 27). Figure 14 is the schematic diagram of the coating deposition model. Generally, small size powders are impossible to apply for conventional plasma spraying process, because it's difficult to feed the powder. When big size powders are used, it will create big defects, as shown in Fig. 14(a). Figure 14(b) is the schematic diagram of this work. The deposition of small size particles is realized by the combination of VLPPS technology and powder design. Due to the long plasma jet, the soft agglomerated powders can be exploded into small ones. Small size deposited particles help to reduce defects, voids, cracks and non-bonded interfaces and improve the density of coatings.

Conclusion

By using VLPPS at 60 kW power, YSZ individual particles were deposited. The morphology and deposition behavior of these particles were analyzed. It is mainly liquid phase deposition between 250 to 450 mm. In the case of 250 mm, the flattened particles were splashed at a low substrate temperature and exhibited a regular disk when the substrate temperature was above 203°C. The flattened particles at different spraying distances (250, 350 and 450 mm) were less than 10 μm. At different spraying distances, there is an approximately linear relationship between the thickness of flattened particles and their diameters. At the same time, the flattened ratio is about 4.7. The width of the cracks is less than 0.02 μm, which is much smaller than that of traditional plasma spraying. The gas permeability of the coatings prepared at 350 mm is 1.5×10^{-7} cm^4 gf^{-1} s^{-1}, which concludes that spraying agglomerated powders by

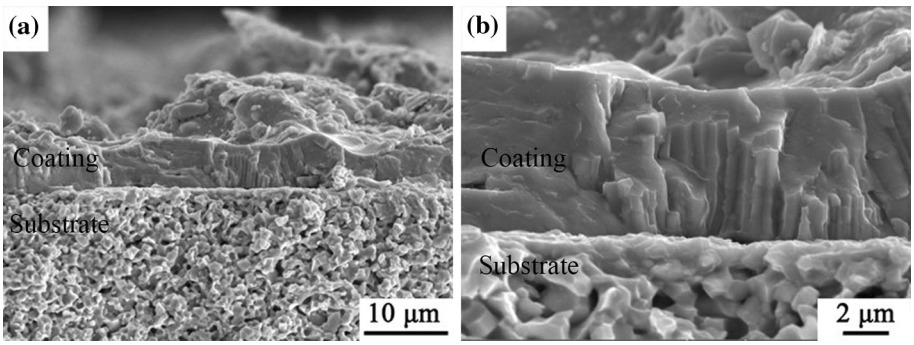

Fig. 13 Fractured cross section of the coating prepared by VLPPS at spraying distance of 350 mm

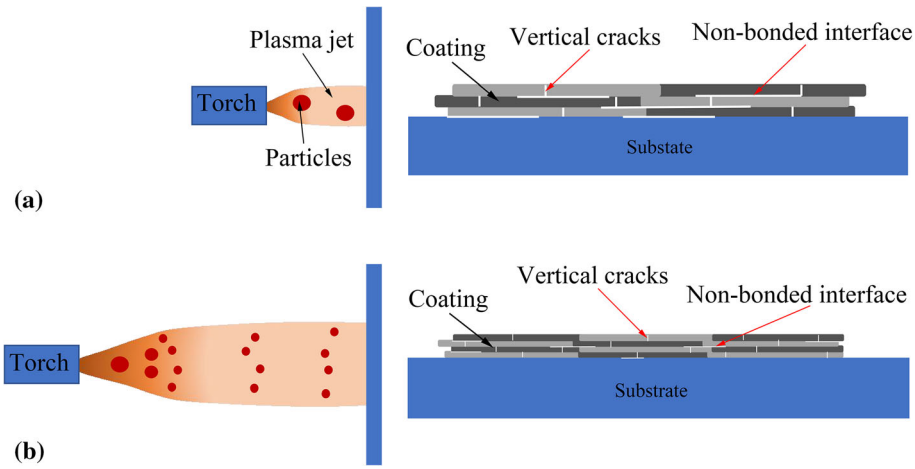

Fig. 14 Schematic diagram of the coating deposition model: (a) conventional plasma spraying; (b) this work

VLPPS is a promising method for preparing thin gastight ceramic coatings.

Acknowledgments This work was supported by the National Key Research and Development Program of China (Basic Research Project, Grant No. 2017YFB0306100), the National Natural Science Foundation of China (Grant No. 91860114), and the National Key Research and Development Program of China (China-USA Intergovernmental Cooperation Project, Grant No. 2017YFE0105900).

References

1. L. Bianchi, P. Lucchese, A. Denoirjean, and P. Fauchais, Zirconia Splat Formation and Resulting Coating Properties, 1995
2. C.C. Berndt, Thermal Spray: A United Forum for Scientific and Technological Advances, the 1st United Thermal Spray Conference, 1997
3. A. Kucuk, R.S. Lima, and C.C. Berndt, Influence of Plasma Spray Parameters on Formation and Morphology of ZrO2-8 wt% Y2O3 Deposits, *J. Am. Ceram. Soc.*, 2001, **84**(4), p 693-700
4. Y.-Z. Xing, C.-J. Li, Q. Zhang, C.-X. Li, and G.-J. Yang, Influence of Microstructure on the Ionic Conductivity of Plasma-Sprayed Yttria-Stabilized Zirconia Deposits, *J. Am. Ceram. Soc.*, 2008, **91**(12), p 3931-3936
5. C.-J. Li, G.-J. Yang, and C.-X. Li, Development of Particle Interface Bonding in Thermal Spray Coatings: A Review, *J. Therm. Spray Technol.*, 2012, **22**(2-3), p 192-206
6. C. Lamuta, G. Di Girolamo, and L. Pagnotta, Microstructural, Mechanical and Tribological Properties of Nanostructured YSZ Coatings Produced with Different APS Process Parameters, *Ceram. Int.*, 2015, **41**(7), p 8904-8914
7. A. Vardelle, C. Moreau, J. Akedo, H. Ashrafizadeh, C.C. Berndt, J.O. Berghaus, M. Boulos, J. Brogan, A.C. Bourtsalas, A. Dolatabadi, M. Dorfman, T.J. Eden, P. Fauchais, G. Fisher, F. Gaertner, M. Gindrat, R. Henne, M. Hyland, E. Irissou, E.H. Jordan, K.A. Khor, A. Killinger, Y.-C. Lau, C.-J. Li, L. Li, J. Longtin, N. Markocsan, P.J. Masset, J. Matejicek, G. Mauer, A. McDonald, J. Mostaghimi, S. Sampath, G. Schiller, K. Shinoda, M.F. Smith, A.A. Syed, N.J. Themelis, F.-L. Toma, J.P. Trelles, R. Vassen, and P. Vuoristo, The 2016 Thermal Spray Roadmap, *J. Therm. Spray Technol.*, 2016, **25**(8), p 1376-1440
8. C. Zhang, H.L. Liao, W.Y. Li, G. Zhang, C. Coddet, C.J. Li, C.X. Li, and X.J. Ning, Characterization of YSZ Solid Oxide Fuel Cells Electrolyte Deposited by Atmospheric Plasma Spraying and Low Pressure Plasma Spraying, *J. Therm. Spray Technol.*, 2006, **15**(4), p 598-603
9. G.-J. Yang, Z.-L. Chen, C.-X. Li, and C.-J. Li, Microstructural and Mechanical Property Evolutions of Plasma-Sprayed YSZ Coating During High-Temperature Exposure: Comparison Study Between 8YSZ and 20YSZ, *J. Therm. Spray Technol.*, 2013, **22**(8), p 1294-1302
10. H. Sun, Y. Chen, F. Chen, Y. Zhang, and M. Liu, High-Performance Solid Oxide Fuel Cells Based on a Thin La0.8Sr0.2-Ga0.8Mg0.2O3−δ Electrolyte Membrane Supported by a Nickel-Based Anode of Unique Architecture, *J. Power Sources*, **301**, 199-203 (2016)
11. P. Alnegren, M. Sattari, J.-E. Svensson, and J. Froitzheim, Temperature Dependence of Corrosion of Ferritic Stainless Steel in Dual Atmosphere at 600-800 C, *J. Power Sources*, 2018, **392**, p 129-138

12. S. Frangini, A. Masi, L.D. Seta, M. Bianco, and J. Van Herle, Composite Cu-LaFeO3Conversion Coatings on a 18Cr Ferritic Stainless Steel for IT-SOFC Interconnects: Effect of Long-Term Air Exposure at 700 C on Cr Diffusion Barrier and Electrical Properties, *J. Electrochem. Soc.*, 2018, **165**(2), p F97-F104
13. N.H. Menzler, D. Sebold, and O. Guillon, Post-Test Characterization of a Solid Oxide Fuel Cell Stack Operated for More Than 30,000 Hours: The Cell, *J. Power Sources*, 2018, **374**, p 69-76
14. M. Bianco, J.P. Ouweltjes, and J. Van herle, Degradation Analysis of Commercial Interconnect Materials for Solid Oxide Fuel Cells in Stacks Operated up to 18000 HOURS, *International Journal of Hydrogen Energy*, **44**(59), 31406-31422 (2019)
15. S. Lee, Y.-H. Jang, H.Y. Shin, K. Lee, M. Bae, J. Kang, and J. Bae, Reliable Sealing Design of Metal-Based Solid Oxide Fuel Cell Stacks for Transportation Applications, *Int. J. Hydrogen Energy*, 2019, **44**(57), p 30280-30292
16. T.A. Prokop, K. Berent, M. Mozdzierz, J.S. Szmyd, and G. Brus, A Three-Dimensional Microstructure-Scale Simulation of a Solid Oxide Fuel Cell Anode—The Analysis of Stack Performance Enhancement After a Long-Term Operation, *Energies*, 2019, **12**(24), p 4784
17. T. Zhu, X. Chen, W. Ni, Q. Zhong, and M. Han, Structural and Electrochemical Property Evolutions of Perovskite SOFC Anodes: Role of Fuel Atmosphere in (La0.4Sr0.6)1-Co0.2Fe0.7Nb0.1O3-δ, *International Journal of Hydrogen Energy*, **44**(59), 31386-31393 (2019)
18. X. He, B. Meng, Y. Sun, B. Liu, and M. Li, Electron Beam Physical Vapor Deposition of YSZ Electrolyte Coatings for SOFCs, *Appl. Surf. Sci.*, 2008, **254**(22), p 7159-7164
19. Y.-Z. Xing, C.-J. Li, C.-X. Li, and G.-J. Yang, Influence of Through-Lamella Grain Growth on Ionic Conductivity of Plasma-Sprayed Yttria-Stabilized Zirconia as an Electrolyte in Solid Oxide Fuel Cells, *J. Power Sources*, 2008, **176**(1), p 31-38
20. Z. Zheng, J. Luo, and Q. Li, Mechanism of Competitive Grain Growth in 8YSZ Splats Deposited by Plasma Spraying, *J. Therm. Spray Technol.*, 2015, **24**(5), p 885-891
21. C.-J. Li, X.-J. Ning, and C.-X. Li, Effect of Densification Processes on the Properties of Plasma-Sprayed YSZ Electrolyte Coatings for Solid Oxide Fuel Cells, *Surf. Coat. Technol.*, 2005, **190**(1), p 60-64
22. H. Tsukuda, A. Notomi, and N. Histatome, Application of Plasma Spraying to Tubular-Type Solid Oxide Fuel Cells Production, *J. Therm. Spray Technol.*, 2000, **9**(3), p 364-368
23. X.-J. Ning, C.-X. Li, C.-J. Li, G.-J. Yang, Effect of Powder Structure on Microstructure and Electrical Properties of Plasma-Sprayed 4.5 mol% YSZ coating, *Vacuum*, **80**(11-12), 1261-1265 (2006)
24. R. Hui, Z. Wang, O. Kesler, L. Rose, J. Jankovic, S. Yick, R. Maric, and D. Ghosh, Thermal Plasma Spraying for SOFCs: Applications, Potential Advantages, and Challenges, *J. Power Sources*, 2007, **170**(2), p 308-323
25. G. Bolelli, L. Lusvarghi, T. Varis, E. Turunen, M. Leoni, P. Scardi, C.L. Azanza-Ricardo, and M. Barletta, Residual Stresses in HVOF-Sprayed Ceramic Coatings, *Surf. Coat. Technol.*, 2008, **202**(19), p 4810-4819
26. J. Kiilakoski, R. Musalek, F. Lukac, H. Koivuluoto, and P. Vuoristo, Evaluating the Toughness of APS and HVOF-Sprayed Al2O3-ZrO2-COATINGS by In SITU- and Macroscopic Bending, *J. Eur. Ceram. Soc.*, 2018, **38**(4), p 1908-1918
27. E.-J. Yang, C.-J. Li, G.-J. Yang, C.-X. Li, and M. Takahashi, Effect of Intersplat Interface Bonding on the Microstructure of Plasma-Sprayed Al_2O_3 Coating, *IOP Conference Series: Materials Science and Engineering*, 2014, **61**, p 012022
28. C.J. Li and W.Z. Wang, Quantitative Characterization of Lamellar Microstructure of Plasma-Sprayed Ceramic Coatings Through Visualization of Void Distribution, *Mater. Sci. Eng., A*, 2004, **386**(1), p 10-19
29. T. Ide, T. Namikawa, and Y. Yamazaki, Preparation of 8 YSZ Thin Films on Porous LSM Substrates by Electron Beam Evaporation, *□□□□□□□□□□□□□□□: denki kagaku*, **64**, (1996)
30. Electron Beam Physical Vapor Deposition of YSZ Electrolyte Coatings for SOFCs, (Accessed 22 254)
31. M. Hartmanová, V. Nádaždy, F. Kundracik, and C. Mansilla, Influence of Deposition Conditions on Electrical and Mechanical Properties of Sm2O3-doped CeO2 Thin Films Prepared by EB-PVD (IBAD) Methods. Part 1: Effective Relative Permittivity, *Applied Surface Science*, **269**, 65-71 (2013)
32. Q.-Y. Chen, X.-Z. Peng, G.-J. Yang, C.-X. Li, and C.-J. Li, Characterization of Plasma Jet in Plasma Spray-Physical Vapor Deposition of YSZ Using a<80 kW Shrouded Torch Based on Optical Emission Spectroscopy, *J. Therm. Spray Technol.*, 2015, **24**(6), p 1038-1045
33. G. Mauer and R. Vaßen, Plasma Spray-PVD: Plasma Characteristics and Impact on Coating Properties, *J. Phys: Conf. Ser.*, 2012, **406**, p 012005
34. L. Zhu, N. Zhang, B. Zhang, R. Bolot, H. Liao, and C. Coddet, In Situ Synthesis of FeAl Dense Coatings by Very Low Pressure Reactive Plasma Spraying, *J. Therm. Spray Technol.*, 2012, **22**(2-3), p 90-95
35. M. Goral, S. Kotowski, A. Nowotnik, M. Pytel, M. Drajewicz, and J. Sieniawski, PS-PVD Deposition of Thermal Barrier Coatings, *Surf. Coat. Technol.*, 2013, **237**, p 51-55
36. K. Iizuka, M. Kambara, and T. Yoshida, Growth of Tin Oxide Thick Films by Plasma Spray Physical Vapor Deposition, *Sensors and Actuators B: Chemical*, 2011, **155**(2), p 551-556
37. D. Zhu, H.T. Lin, Y. Zhou, S. Widjaja, and D. Singh, Plasma Spray-Physical Vapor Deposition (PS-PVD) of Ceramics for Protective Coatings, John Wiley & Sons, Inc., 2011
38. G. Mauer, A. Hospach, and R. Vaßen, Process Development and Coating Characteristics of Plasma Spray-PVD, *Surf. Coat. Technol.*, 2013, **220**, p 219-224
39. C.-J. Li and J.-L. Li, Evaporated-Gas-Induced Splashing Model for Splat Formation During Plasma Spraying, *Surf. Coat. Technol.*, 2004, **184**(1), p 13-23
40. A.T.T. Tran, M.M. Hyland, T. Qiu, B. Withy, and B.J. James, Effects of Surface Chemistry on Splat Formation During Plasma Spraying, *J. Therm. Spray Technol.*, 2008, **17**(5-6), p. 637-645
41. M. Vardelle, A. Vardelle, A.C. Leger, P. Fauchais, and D. Gobin, Influence of Particle Parameters at Impact on Splat Formation and Solidification in Plasma Spraying Processes, *Journal of Thermal Spray Technology*, **4**(1), 50-58
42. S. Brossard, P.R. Munroe, A.T.T. Tran, and M.M. Hyland, Study of the Splat Formation for Plasma Sprayed NiCr on Aluminum Substrate as a Function of Substrate Condition, *Surf. Coat. Technol.*, 2010, **204**(16-17), p 2647-2656
43. M. Mutter, G. Mauer, R. Mücke, O. Guillon, and R. Vaßen, Correlation of Splat Morphologies with Porosity and Residual Stress in Plasma-Sprayed YSZ Coatings, *Surf. Coat. Technol.*, 2017, **318**, p 157-169
44. P. Fauchais, M. Vardelle, and S. Goutier, Latest Researches Advances of Plasma Spraying: From Splat to Coating Formation, *J. Therm. Spray Technol.*, 2016, **25**(8), p 1534-1553
45. J.-J. Tian, S.-W. Yao, X.-T. Luo, C.-X. Li, and C.-J. Li, An Effective Approach for Creating Metallurgical Self-bonding in Plasma-Spraying of NiCr-Mo Coating by Designing Shell-Core-Structured Powders, *Acta Mater.*, 2016, **110**, p 19-30
46. X. Jiang and S. Sampath, Effect of Substrate Condition on Splat Formation During Thermal Spray Deposition, *TMS Annual Meeting*, 1998, **1998**, p 439-448
47. S. Sampath, X.Y. Jiang, J. Matejicek, A.C. Leger, and A. Vardelle, Substrate Temperature Effects on Splat Formation,

Microstructure Development and Properties of Plasma Sprayed Coatings Part I: Case Study for Partially Stabilized Zirconia, *Mater. Sci. Eng., A*, 1999, **272**(1), p 181-188

48. C. Delbos, J. Fazilleau, V. Rat, J.F. Coudert, P. Fauchais, and B. Pateyron, Phenomena Involved in Suspension Plasma Spraying Part 2: Zirconia Particle Treatment and Coating Formation, *Plasma Chem. Plasma Process.*, 2006, **26**(4), p 393-414
49. A. Joulia, G. Bolelli, E. Gualtieri, L. Lusvarghi, S. Valeri, M. Vardelle, S. Rossignol, and A. Vardelle, Comparing the Deposition Mechanisms in Suspension Plasma Spray (SPS) and Solution Precursor Plasma Spray (SPPS) Deposition of Yttria-Stabilised Zirconia (YSZ), *J. Eur. Ceram. Soc.*, 2014, **34**(15), p 3925-3940
50. C. Zhang, A.-F. Kanta, C.-X. Li, C.-J. Li, M.-P. Planche, H. Liao, and C. Coddet, Effect of In-Flight Particle Characteristics on the Coating Properties of Atmospheric Plasma-Sprayed 8 mol% Y2O3-ZrO2 Electrolyte Coating Studying by Artificial Neural Networks, *Surf. Coat. Technol.*, 2009, **204**(4), p 463-469
51. Y.Z. Xing, Y. Li, C.J. Li, C.X. Li, and G.J. Yang, Influence of Substrate Temperature on Microcracks Formation in Plasma-Sprayed Yttria-Stabilized Zirconia Splats, *Key Eng. Mater.*, 2008, **373-374**, p 69-72
52. L. Chen, G.-J. Yang, C.-X. Li, and C.-J. Li, Edge Effect on Crack Patterns in Thermally Sprayed Ceramic Splats, *J. Therm. Spray Technol.*, 2016, **26**(3), p 302-314
53. H. Xie, Y.-C. Xie, G.-J. Yang, C.-X. Li, and C.-J. Li, Modeling Thermal Conductivity of Thermally Sprayed Coatings with Intrasplat Cracks, *J. Therm. Spray Technol.*, 2013, **22**(8), p 1328-1336
54. L.I. Changjiu, A. Ohmori, and R. Mcpherson, The Relationship Between Microstructure and Young's Modulus of Thermally Sprayed Ceramic Coatings, *J. Mater. Sci.*, 1997, **32**(4), p 997-1004
55. D. Waldbillig and O. Kesler, Effect of Suspension Plasma Spraying Process Parameters on YSZ Coating Microstructure and Permeability, *Surf. Coat. Technol.*, 2011, **205**(23-24), p 5483-5492